Materials Research Bulletin 48 (2013) 4526–4530

Contents lists available at ScienceDirect

Materials Research Bulletin

journal homepage: www.elsevier.com/locate/matresbu

Preparation of NiMo/γ-Al_2O_3 catalysts with large pore size for vacuum residue hydrotreatment

Guangci Li [a,b], Xinlu Lu [a], Zhe Tang [a], Yunqi Liu [a,*], Xuebing Li [b], Chenguang Liu [a]

[a] State Key Laboratory of Heavy Oil Processing, Key Laboratory of Catalysis, CNPC, China University of Petroleum, Qingdao 266580, PR China
[b] Qingdao Institute of Bioenergy and Bioprocess Technology, Chinese Academy of Science, Qingdao 266101, PR China

ARTICLE INFO

Article history:
Received 6 November 2012
Received in revised form 11 July 2013
Accepted 21 July 2013
Available online 29 July 2013

Keywords:
A. Oxides
A. Nanostructures
B. Crystal growth
D. Catalytic properties

ABSTRACT

γ-Al_2O_3 supports with large pore size were prepared by using rod-like ammonium aluminum carbonate hydroxide (AACH) as precursors. The textural properties of supports are dependent on the different crystallinity of the as-prepared AACH. For investigating their catalytic performance, NiMo/γ-Al_2O_3 hydrotreating catalysts were prepared by loading NiMo oxides on the supports and tested by using vacuum residue as reactant, and the results show that both pore structure and surface acid property of catalysts have significant influences on the catalytic activities for the hydrogenation and the removal of heteroatoms.

1. Introduction

Because of continued depletion of conventional crude oil, new resources are exploited for future energy supplies, such as biomass, to fulfill the increasing worldwide energy consumption [1–3]. Currently, however, biofuels merely act as a supplement which cannot replace fossil fuels for the primary energy production. Thus, how to efficiently process and utilize existing petroleum resource, especially in heavy oil, has attracted intensive attentions. Since high contents of asphaltenes and metals (mainly Ni, V) exist in heavy oil, the catalysts deactivate predominantly due to the pore blocking resulted from the deposition of metal poisoners, heteroatoms and asphaltenes [4,5], which increases the difficulty of hydroprocessing heavy oil [6,7]. For avoiding this problem to enhance the activity and prolong the life of catalysts, the supports with relatively large pore size are required.

Generally, γ-Al_2O_3 is a common hydrotreating catalyst support due to its special physicochemical properties and low cost [8–10]. However, traditional alumina usually has a broad pore size distribution, and the pore size is below 10 nm, which limits their catalytic applications in residue hydrotreating. Ammonium aluminum carbonate hydroxide (AACH, with formula $NH_4Al(OH)_2CO_3$) is constructured of the $AlO_2(OH)_4$ chains of octahedra combined with NH_4^+ and CO_3^{2-} groups [11–13]. Heated at high temperature, AACH can be transformed to γ-Al_2O_3. During this process, large amount of gas molecules (NH_3, CO_2, and H_2O) are released, resulting in lots of mesopores and macropores in the inter- and intra-particles. Thus, it can be used as a promising precursor to prepare alumina support with large pore size and volume.

Herein, we prepared NiMo/γ-Al_2O_3 hydrotreating catalysts by using two types of AACH as the precursor of alumina supports, and then examined their catalytic activities for vacuum residue. It is found that the catalysts derived from AACH exhibit relatively high hydrogenation activity for vacuum residue.

2. Experimental

2.1. Preparation of γ-Al_2O_3 supports

This process has been described previously in detail [14]. Firstly, 5.0 g of aluminum hydroxide xerogel (AHx) (Henghui Chemical Engineering Co., Ltd., Shandong, China) was mixed with a 60 ml aqueous solution of NH_4HCO_3, and the molar ratio of NH_4HCO_3/Al was fixed at 7.0:1. The pH value of this system was adjusted to be 10.5 using aqueous $NH_3{\cdot}H_2O$. Secondly, the final mixture was transferred into 100 ml TEFLON-lined stainless autoclave and kept at 105 °C for 48 h. After that, white precipitate was collected and washed with deionized water for several times, and then dried under vacuum at 60 °C for 8 h. Thirdly, the obtained dried precipitate was mixed with aqueous acetic acid solution (20.0 wt.%) and then extruded into cylindrical particles with the diameter of 1.6 mm. Finally, the extrudate was calcined in static air at 600 °C for 2 h. The obtained alumina support was denoted as "A-1".

* Corresponding author. Tel.: +86 532 86981861; fax: +86 532 86981787.
E-mail address: liuyq@upc.edu.cn (Y. Liu).

0025-5408/$ – see front matter © 2013 Elsevier Ltd. All rights reserved.
http://dx.doi.org/10.1016/j.materresbull.2013.07.041

In addition, we used alumina (obtained by calcining the above AHx at 500 °C for 2 h) as reactant instead of AHx, and then a similar alumina support was prepared. This support was denoted as "A-2". For comparison, a commercial alumina support (Condea Chemical Co., Germany) was selected as a reference, donated as A-ref.

2.2. Preparation of catalysts

The catalysts were prepared by incipient wetness impregnation of alumina supports with an aqueous solution containing ammonium heptamolybdate ($(NH_4)_6Mo_7O_{24}{\cdot}4H_2O$) and nickel nitrate ($Ni(NO_3)_2{\cdot}6H_2O$). The loading quantity of NiO and MoO_3 was controlled to be 0.36 wt.% and 4.8 wt.%, respectively. The impregnated supports were dried overnight in air at 80 °C and calcined at 500 °C for 3 h. The corresponding catalysts were labeled as C-1, C-2, and C-ref, respectively.

2.3. Characterization

The crystal structure of the products was detected on a Panalytical X'Pert Pro MPD X-ray diffractometer (Netherlands) using CuKα radiation of wavelength 1.5406 ?. The crystallite size of aluminas was calculated through Scherrer formula ($D = 0.9\lambda/\beta\cos\theta$, where D, λ, β, and θ are crystallite size, wavelength, full width at half-maximum intensity of diffraction peaks in radians, and Bragg's diffraction angle, respectively). The morphology was observed on a JEM-2100UHR transmission electron microscopy (Japan) with an accelerating voltage of 200 kV. The pore structures of catalysts were measured through N_2 adsorption–desorption isotherms on a Micromeritics Tristar II 3020 surface area analyzer and mercury intrusion method on a Micromeritics AUTOPORE 9500 porosimeter (USA), respectively. The acidity of the catalysts was examined byNH_3-TPD (temperature-programmed desorption) measurements on a Quantachrome CHEMBET-3000 instrument (USA). Additionally, H_2-TPR measurement of catalysts was also conducted on this device. ^{27}Al MAS NMR spectra were acquired on a Bruker Avance 300 spectrometer (Switzerland).

2.4. Activity test

The catalytic activity was tested in a tank reactor. 1.25 g of fresh catalyst was sulfided in situ for each activity test. In this stage, 10.0 g of vacuum residue from Saudi Arabian light crude was diluted with 35.0 g of toluene. The resultant mixture was charged into the reactor (100 ml capacity), and then 0.4 g of CS_2 was added with fresh catalyst. The reactor was purged five times with H_2 to exchange the air inside. The reaction mixture was heated to the required temperature at a heating ramp of 3 °C/min. A two-step temperature-raising process was applied so that the fresh catalyst can be sulfided sufficiently. The sulfiding conditions were as follows: H_2 initial pressure, 4.0 MPa; temperature, 200 °C for 4 h and 300 °C for 2 h; stirring speed, 750 rpm.

Afterwards, the reactor was cooled down to room temperature quickly. The reactor was then purged with H_2 to remove gas impurities, and then heated to the reaction temperature. The reaction conditions were as follows: H_2 initial pressure, 7.0 MPa; temperature, 380 °C for 2 h; stirring speed, 750 rpm. Products were separated from the catalyst, and their components were analyzed with an Analytik Jena CONTRAA 700 atomic absorption spectrometer.

3. Results and discussion

3.1. Crystalline structure

Fig. 1a shows the XRD patterns of fresh samples derived from AHx and alumina. It was found that the diffraction peaks of the two

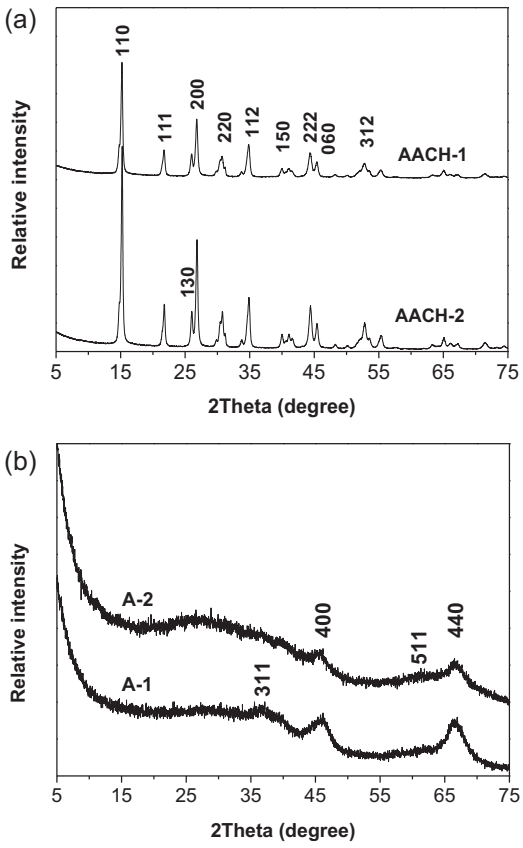

Fig. 1. XRD patterns of (a) fresh and (b) calcined samples derived from AHx and alumina.

samples can be indexed to the $NH_4Al(OH)_2CO_3$ phase (JCPDS 01-076-1923). However, their crystallite sizes are different according to the relative intensity of diffraction peaks. The size of AACH-2 (arises from alumina) is larger than that of AACH-1 (arises from AHx). For instance, the crystallite sizes of AACH-2 and AACH-1 were estimated from the half-width of the (1 1 0) diffraction peak by using Sherrer equation, and the corresponding values are 43.6 and 25.8 nm respectively. This may be due to that the crystallite size of alumina is smaller than that of AHx. During hydrothermal process, the dissociation and hydration of alumina generated many $Al(OH)_3$ nanocrystallites with relatively small size. These nanocrystallites possess higher surface energy, which improves their reaction with NH_4HCO_3 and the formation of well-crystallized AACH-2.

After calcination, the two AACH can transform into γ-Al_2O_3 (JCPDS 00-010-0425). Due to the removal of NH_4^+ and CO_3^{2-} groups combined with $AlO_2(OH)_4$ chains during the decomposition of AACH, large amounts of spaces between $AlO_2(OH)_4$ layers were generated, and thus the layer structures were destroyed, leading to aluminas with weak crystallinity.

3.2. Morphology

The morphologies of the as-prepared AACH and corresponding alumina are shown in Fig. 2. Two AACH samples are composed of rod-like particles with large aspect ratio. After calcination, rod-like morphology was preserved, suggesting their excellent thermal stability. Because of the decomposition of AACH, large amounts of mesopore with small size appeared in intra-particles, as shown in Fig. 2, inset. Moreover, the diameter of AACH-1 rod-like particles is larger than that of AACH-2. It is believed that the porosity of

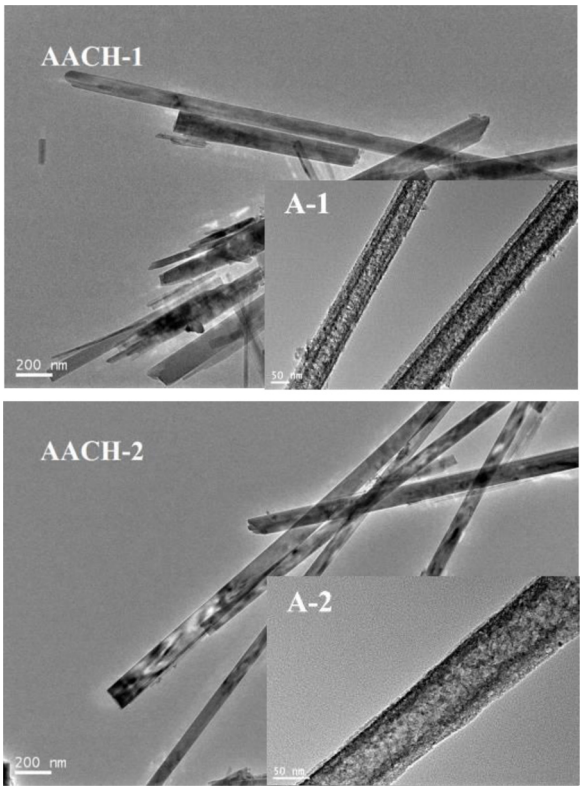

Fig. 2. TEM images of the two AACH and alumina samples (inset).

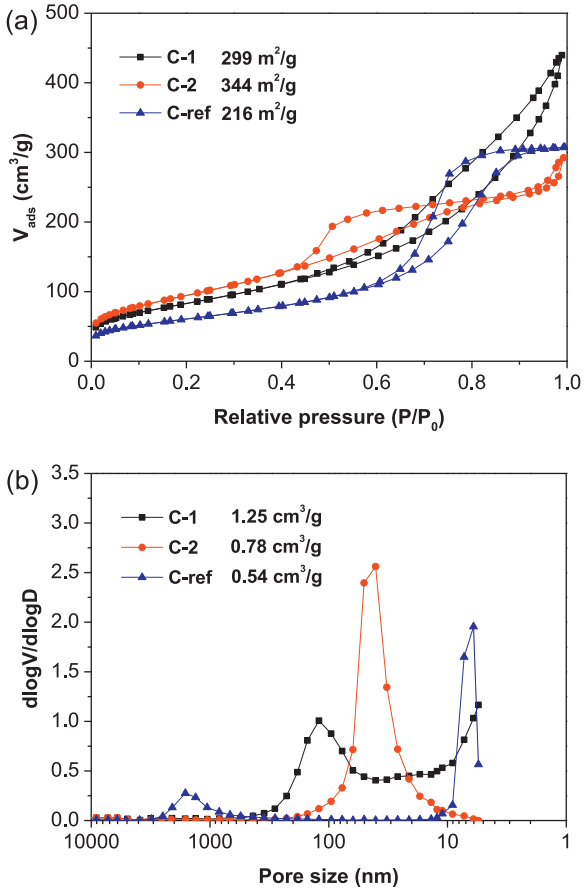

Fig. 3. Pore structure of the catalysts. (a) N_2 adsorption–desorption isotherms and their specific surface area; (b) pore size distribution and pore volume from mercury intrusion curves.

alumina materials mainly derived from the space between adjacent particles. Large particles are favorable to form larger pores. Thus, the pore volume of support A-1 is relatively large (see Table S1 in Supplementary data).

3.3. Textural properties

The textural properties of the three catalysts were detected with N_2-sorption measurement, and the results are shown in Fig. 3a. It can be seen that their isotherms types are different. For catalyst C-1, the isotherms are of type II, suggesting the presence of large mesopores or macropores. For catalyst C-2, the adsorption process has two steps, which means that the porosity exhibits a bimodal distribution. The adsorption quantity increases rapidly when the relative pressure (p/p_0) exceeds 0.8. The shape of this part is similar to that of C-1, which indicates that C-2 also has large mesopores or maropores. The isotherms for catalyst C-ref are of type IV, which is characteristic of mesoporous material. According to our previous results [14], the relatively high specific surface areas (SSA) of support A-1 and A-2 are attributed to the decomposition of AACH. Since AACH with higher crystallinity may release more gas molecules per unit mass (see Fig. S1 in Supplementary data), the SSA of support A-2 is higher than that of A-1 as well as the corresponding catalysts.

To further investigate and characterize the larger mesopores and macropores of the three catalysts, mercury intrusion measurements were carried out, as shown in Fig. 3b. Apparently, their pore volume decreases in order. The pore size of catalyst C-2 and C-ref mainly locates at 40 and 6 nm, respectively. Catalyst C-1 has two types of pores, small pores with 5.5 nm; large pore beyond 100 nm. The size of AACH-2 particles is more uniform than that of AACH-1, which leads to a narrow pore size distribution for catalyst C-2.

3.4. Acidity of catalysts

Fig. 4 shows the NH_3-TPD curves of catalysts. Only one peak at ~180 °C was found in all the curves, which leads to the assumption that only weak acid sites exist in the three catalysts. Considering that the amount of active components loading on the supports is low, and only Lewis acid sites exist on the surface of alumina [15], most of acid sites on catalyst surface belong to Lewis acid site. Furthermore, the peak area under the TPD curves represents adsorption quantity of NH_3, and thus the total acid amount of

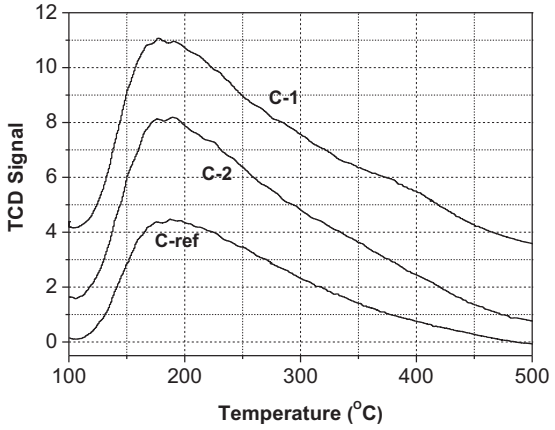

Fig. 4. NH_3-TPD curves of the as-prepared catalysts.

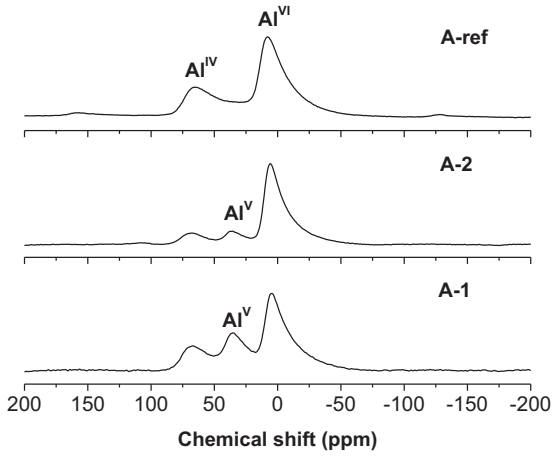

Fig. 5. ^{27}Al MAS NMR spectra of the supports.

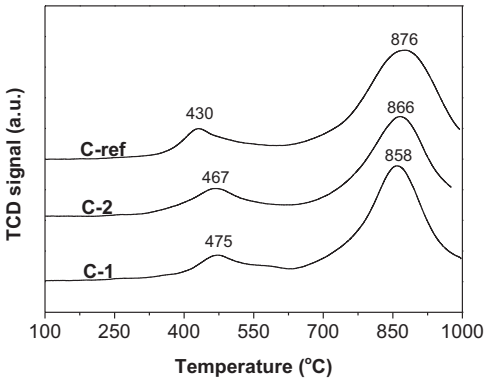

Fig. 6. H_2-TPR curves of the as-prepared catalysts.

catalyst C-1 and C-2 is higher than that of C-ref. Because of the same loading amounts of active components, these additional acid sites are contributed by the supports.

Fig. 5 shows the ^{27}Al MAS NMR spectra of three supports. It is evident that both support A-1 and A-2 contain five-coordinated aluminums [16], but not for A-Ref. This is related to the poor crystallinity of A-1 and A-2, because five-coordinated aluminum is considered to be present in alumina's amorphous domains [17]. The population of different AlO_x species can be estimated by fitting Lorentzian lines to each peaks and calculating the area under the peaks. For A-1 and A-2, the populations of AlO_5 species are 17.6% and 7.2%, respectively. Since the coordinately unsaturated surface (CUS) aluminum cations are the origin of Lewis acid sites locating on the surface of alumina, we believed that the additional acid sites of catalyst C-1 and C-2 arise from five-coordinated aluminum of supports; in addition, A-1 could supply more Lewis acid sites than A-2.

For further understanding the effect of support on the interactions between Ni, Mo and the supports, H_2-TPR measurements were carried out, as shown in Fig. 6. All catalysts exhibit similar TPR curve, which has two reduction peaks in 400–900 °C region. The first peak at low temperature can be attributed to the partial reduction of Mo^{6+} to Mo^{4+} of amorphous and defective Mo oxides [18,19]. The second peak in high temperature region comprises the deep reduction of all Mo species, including highly dispersed tetrahedral Mo species [20,21]. The loading amount of Ni is very low, therefore the reduction peak of Ni species cannot be observed. Comparing the three curves, the reduction peaks for Mo species shifted to lower temperature gradually (876 °C > 866 °C > 858 °C), indicating that there are more easily reducible Mo species in the C-1 and C-2. The results also suggest that the interaction between the Mo species and the as-prepared supports is weaker than that between the Mo species and reference support. This will affect the transformation of Mo species from oxidic state to sulfidic state and subsequent hydrogenation activity.

3.5. Catalytic activity

The hydrotreating activities of catalysts were studied for vacuum residue from Saudi Arabian light crude, and the test results are listed in Table 1. It can be seen that both catalyst C-1 and C-2 exhibited better hydrogenation capability than C-ref according to the ratio of H/C of corresponding products after reaction. It has been reported that Lewis acid site is crucial to the hydrogenation of olefin and aromatic ring [22–24], thus the hydrogenation capability of catalyst C-1 and C-2 is better than that of C-ref. This is also relative to the interaction between Mo species and support. Based on the TPR results, this interaction for C-ref is stronger than that for C-1 and C-2. Stronger interaction may limit the transformation of Mo species from oxidic state to sulfidic state, which will consequently lower the hydrogenation activity of catalyst.

In terms of heteroatoms removal, the catalysts C-1 and C-2 exhibit an obvious advantage relative to C-ref. This is mainly attributed to their more acid sites and larger porosity, which are favorable for the diffusion and conversion of large residue molecules containing heteroatoms. For C-1 and C-2, although the hydrogenation capability of C-1 is better than that of C-2 as mentioned above, the activity, especially hydrodemetallization performance of catalyst C-1 is lower than that of C-2. Thus, it was believed that this difference is related to their surface area and pore size. The intrinsic activity of the hydrodemetallization catalyst is proportional to its surface area [25]. High surface area favors the adsorption and deposition of metal on the catalyst. Besides, large pore size can increase diffusion rate of residue molecules in the catalyst, which protects the porosity from blocking. Comparing the two catalysts, C-2 possesses larger surface area and pore size. Despite there are pores larger than 100 nm in the C-1, the pores less than 5 nm are still predominant, whereas most of pores of C-2 centralizes on 40 nm. As a result, C-2 exhibits relatively excellent hydrogenation performance.

This work indicates that an optimal activity for catalysts is a combination of proper textural properties and surface acidity. Furthermore, removing heteroatoms depends simultaneously on the hydrogenation and hydrogenolysis active sites of catalyst. Thus, to further improve hydrotreating performance, more active components are required.

Table 1
The properties of feedstock before and after reaction.

Property	Feedstock	C-1	C-2	C-ref	Removal percentage	C-1	C-2	C-ref
Ratio of H/C	1.422	1.454	1.441	1.429				
S (wt.%)	4.64	4.14	3.91	4.54	S%	10.8	15.7	2.2
N (wt.%)	0.32	0.22	0.23	0.31	N%	31.3	28.1	3.1
Ni (μg/g)	31.0	22.9	17.0	25.2	Ni%	26.1	45.2	18.7
V (μg/g)	59.8	29.4	18.1	33.0	V%	50.8	69.7	44.8

4. Conclusion

In this study, NiMo/γ-Al_2O_3 hydrotreating catalysts with large pore size were prepared by loading NiMo oxides on rod-like alumina supports, and their hydrogenating performances toward vacuum residue were investigated. The results indicate that more AlO_5 species may induce more Lewis acid sites that are favorable for the hydrogenation of residue molecules. The weak interaction between Mo species and support is propitious to the sulfuration of Mo species, which promotes hydrogenation reaction. In addition, large mesopore and high surface area are favorable for the removal of heteroatoms, particularly for Ni and V. Since the supports obtained here possess large porosity and high SSA, they display a good application prospect for heavy oil upgrading.

Acknowledgements

Financial support from the National Natural Science Foundation, China (No. 21176258, U1162203), and Specialized Research Fund for the Doctoral Program of Higher Education, "SRFDP" 20110133110002 are gratefully acknowledged.

Appendix A. Supplementary data

Supplementary material related to this article can be found, in the online version, at http://dx.doi.org/10.1016/j.materresbull.2013.07.041.

References

[1] H.N. Bhatti, M.A. Hanif, M. Qasim, Ata-ur-Rehman, Fuel 87 (2008) 2961.
[2] B. Delfort, I. Durand, G. Hillion, A. Jaecher-Voirol, X. Montagne, Oil Gas Sci. Technol-Rev IFP 63 (2008) 395.
[3] J.S. Dennis, S.A. Scott, A.L. Stephenson, Process Saf. Environ. Protect 86 (2008) 427.
[4] B.G. Johnson, F.E. Massoth, J. Bartholdy, AIChE J. 32 (1986) 1980.
[5] E. Furimsky, F.E. Massoth, Catal. Today 52 (1999) 381.
[6] K. Rajagopalan, D. Luss, Ind. Eng. Chem. Process Des. Dev. 18 (1979) 459.
[7] S.Y. Lee, J.D. Seader, C.H. Tsai, F.E. Massoth, Ind. Eng. Chem. Res. 30 (1991) 29.
[8] C. Misra, Industrial Alumina Chemicals, ACS Monograph 184, American Chemical Society, Washington, DC, 1986.
[9] G. Tournier, M. Lecroix-Repellin, G.M. Pajonk, Stud. Surf. Sci. Catal. 31 (1987) 333.
[10] H. Topsøe, B.S. Clausen, F.E. Massoth, Hydrotreating Catalysis, Springer, Berlin, 1996.
[11] A.J. Frueh, J.P. Golightly, Can. Mineral 9 (1967) 51.
[12] E. Corazza, C. Sabelli, S. Vannucci, Neues Jahrb. Mineral. Monatsh. 9 (1977) 381.
[13] S. Kato, T. Iga, S. Hatano, Y. Isawa, J. Ceram. Soc. Jpn. 84 (1976) 215.
[14] G. Li, Y. Liu, L. Guan, X. Hu, C. Liu, Mater. Res. Bull. 47 (2012) 1073.
[15] S. Roy, G. Mpourmpakis, D.-Y. Hong, D.G. Vlachos, A. Bhan, R.J. Gorte, ACS Catal. 2 (2012) 1846.
[16] S. Acosta, R.J.P. Corriu, D. Leclercq, P. Lefèvre, P.H. Mutin, A. Vioux, J. Non-Cryst. Solids 170 (1994) 234.
[17] S.A. Bagshaw, T.J. Pinnavaia, Angew. Chem. Int. Ed. 35 (1996) 1102.
[18] M. Henker, K.-P. Wendlandt, J. Valyon, P. Bornmann, Appl. Catal. 69 (1991) 205.
[19] M.A. Domínguez-Crespo, A.M. Torres-Huerta, L. Díaz-García, E.M. Arce-Estrada, E. Ramírez-Meneses, Fuel Process. Technol. 89 (2008) 788–798.
[20] R. López Cordero, A. López Agudo, Appl. Catal. A: Gen. 202 (2000) 23–35.
[21] D. Ferdous, A.K. Dalai, J. Adjaye, Appl. Catal. A: Gen. 260 (2004) 153–162.
[22] C.E. Volckmar, M. Bron, U. Bentrup, A. Martin, P. Claus, J. Catal. 261 (2009) 1.
[23] J. Fontana, C. Vignado, E. Jordão, W.A. Carvalho, Chem. Eng. J. 165 (2010) 336.
[24] M.F. Williams, B. Fonfé, C. Woltz, A. Jentys, J.A.R. van Veen, J.A. Lercher, J. Catal. 251 (2007) 497.
[25] Y.-W. Chen, W.-C. Hsu, Ind. Eng. Chem. Res. 36 (1997) 2526.